



Cite this: DOI: 10.1039/d0cs00084a

## Acceptor–donor–acceptor type molecules for high performance organic photovoltaics – chemistry and mechanism†

 Xiangjian Wan,<sup>id</sup>abc Chenxi Li,<sup>a</sup> Mingtao Zhang<sup>id</sup>a and Yongsheng Chen<sup>id</sup>\*abc

The study of organic photovoltaics (OPVs) has made great progress in the past decade, mainly attributed to the invention of new active layer materials. Among various types of active layer materials, molecules with A–D–A (acceptor–donor–acceptor) architecture have demonstrated much great success in recent years. Thus, in this review, we will focus on A–D–A molecules used in OPVs from the viewpoint of chemists. Notably, the chemical structure–property relationships of A–D–A molecules will be highlighted and the underlying reasons for their outstanding performance will be discussed. The device stability correlated to A–D–A molecules will also be commented on. Finally, an outlook and challenges for future OPV molecule design and device fabrication to achieve higher performance will be presented.

Received 3rd February 2020

DOI: 10.1039/d0cs00084a

[rsc.li/chem-soc-rev](http://rsc.li/chem-soc-rev)

### 1. Introduction

Among many alternative energy technologies such as wind, nuclear, biomaterial energy, *etc.*, photovoltaic cells have always been regarded as one of the most promising strategies to address energy and environment issues. Indeed, organic photovoltaics (OPVs) have been thought to have many advantages such

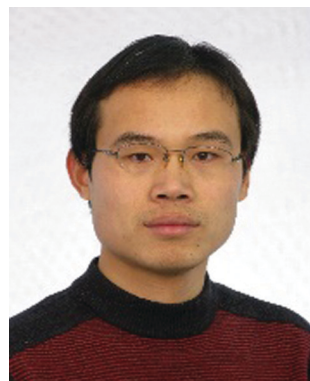
as low cost, light weight, flexibility, semi-transparency, *etc.*<sup>1</sup> Presently, a remarkable power conversion efficiency (PCE) of over 16–18% has been achieved for OPV devices in labs.<sup>2–7</sup> It has been a long journey for OPVs from the initial PCE of 1% to the present level of about 18%, in which chemists have played a great role by creating new and better organic active layer materials that have had a direct and significant impact on the improvement of PCEs in recent years (Fig. 1a). In 1986, Tang reported the pioneering work on OPVs, in which a two-layer organic photovoltaic cell (Fig. 1b) was fabricated using copper phthalocyanine and a perylene tetracarboxylic derivative and merely gave a PCE of 1%.<sup>8</sup> But the field initially advanced slowly, mainly limited by the absence of effective active layer molecules. The first breakthrough came in 1995, when the bulk heterojunction (BHJ) architecture (Fig. 1c) was invented and soluble fullerene derivative

<sup>a</sup> Key Laboratory of Functional Polymer Materials and the Centre of Nanoscale Science and Technology, Institute of Polymer Chemistry, College of Chemistry, Nankai University, Tianjin 300071, China. E-mail: yschen99@nankai.edu.cn

<sup>b</sup> State Key Laboratory of Elemento-Organic Chemistry, Nankai University, Tianjin, 300071, China

<sup>c</sup> Renewable Energy Conversion and Storage Center (RECAST), Nankai University, Tianjin 300071, China

† Electronic supplementary information (ESI) available: See DOI: 10.1039/d0cs00084a


**Xiangjian Wan**

*Xiangjian Wan received his PhD degree in Organic Chemistry from Nankai University, China, in 2006. Currently, he is a professor of Chemistry, Nankai University. His research interests focus on organic functional material design and application, especially on OPV material design and device optimization.*


**Chenxi Li**

*Chenxi Li received his PhD degree in Organic Chemistry from Nankai University, China, in 1990. Currently, he is a professor of Chemistry, Nankai University. His research interests focus on organic functional material design and synthesis.*

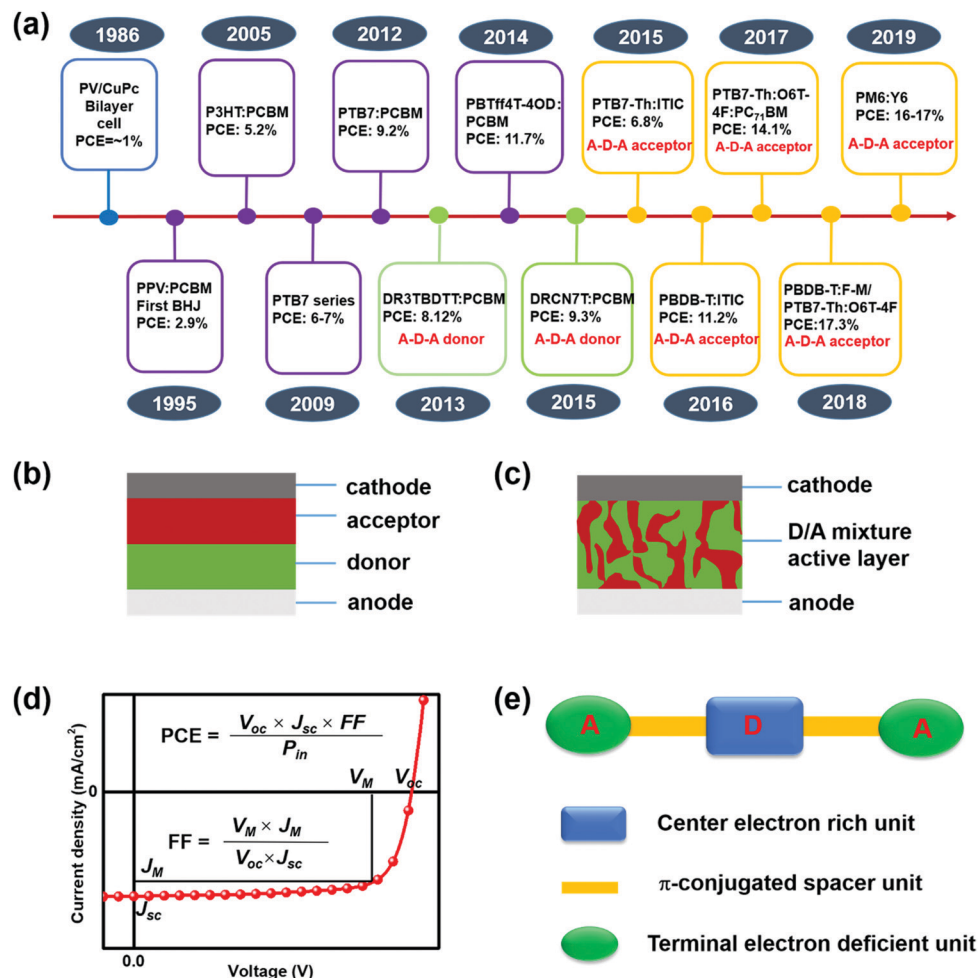


**Fig. 1** (a) A short timeline of major OPV developments from the perspective of active layers. Device structures of (b) planar heterojunction and (c) bulk heterojunction (BHJ) organic photovoltaics. (d) A typical J–V curve of an OPV device indicating the meaning of  $J_{sc}$ ,  $V_{oc}$ , FF and PCE. The voltage and current density at the maximum power point are denoted as  $J_M$  and  $V_M$ . (e) Schematic diagram of general A–D–A molecules.

PCBM was used as the acceptor.<sup>9,10</sup> With high electron affinity and excellent isotropic electron-transport capability, PCBM has since been widely used as the standard acceptor in BHJ OPVs for many years. Following this improvement, OPVs left their decade of silence and stepped into a fast development stage. With PCBM

as the acceptor, the design and synthesis of donor materials have become the main task and focus. Poly(*p*-phenylenevinylene) (PPV) derivatives such as MEH-PPV and MDMO-PPV were the first generation donor materials in BHJ solar cells. But their large bandgaps limited the device current and only around 3% PCEs



**Mingtao Zhang**

*Mingtao Zhang received his PhD degree from Nankai University in 2004. Currently, he is an associate professor in College of Chemistry, Nankai University. His research interests focus on Molecular Modeling and Cheminformatics & Computational Chemistry.*



**Yongsheng Chen**

*Prof. Yongsheng Chen received his PhD in Chemistry from the University of Victoria in 1997. Since 2003, he has been a Chair Professor at Nankai University. His main research interests focus on carbon based nano materials and organic functional materials for green energy applications.*

could be obtained.<sup>11</sup> Later on, a star donor polymer regioregular poly(3-hexylthiophene) (P3HT) was applied and thus much improved PCEs of around 5% were achieved.<sup>12</sup> This works as a strong catalyst since it demonstrated that the great potential of OPVs could be achieved through donor material design and modulation. Following this, various low bandgap donor polymers have been designed, among which PTB7 and its derivatives are probably the most famous and representative ones.<sup>13,14</sup> Meanwhile, in view of the no batch to batch issue, together with the easiness of control of properties, small molecules or oligomer like molecules with definite structures have drawn great attention. Varieties of molecules with definite structures have been designed and evaluated for OPV devices.<sup>15,16</sup> Among them, molecules with A–D–A architectures (Fig. 1e) have demonstrated great success.<sup>17</sup> With fullerene derivatives as the acceptors, A–D–A donor small molecules achieved PCEs of over 10%, which were comparable to the corresponding polymer based cases.<sup>18,19</sup> In the last five years, the design strategy of A–D–A donor molecules has been further successfully used to explore non fullerene acceptors (NFAs), and many A–D–A acceptors have been designed and demonstrated to have excellent device performance.<sup>20–25</sup> The record PCEs in the OPV field for A–D–A molecule based devices have been updated very frequently in the past few years. This latest rapid development is truly remarkable, particularly when we note that studies in OPVs have been ongoing for over half a century and progress during the first few decades had been relatively slow. Presently, efficiencies of 17–18% have been achieved for A–D–A molecule based devices.<sup>2,3,5</sup> These results also indicate that more significant and exciting discoveries in the OPV field have yet to be achieved.

While other types of molecules with defined structures such as D–A–D type molecules developed systematically by Bazan *et al.* have demonstrated decent performance,<sup>26,27</sup> A–D–A molecules have been proven to have better performance than other types of small molecules in the OPV field. This indicates that the unique A–D–A chemical structure should definitely play a major role. Thus, in this tutorial review, we will focus on the A–D–A molecules used in OPVs in the eyes of a chemist. Firstly, a calculation analysis will be given for the frontier electronic band structure and electron density distribution for various types of OPV molecules, which will allow us to have a better understanding of these molecules and the definition of A–D–A molecules. Then, a brief development history of A–D–A molecules for application in OPVs will be given. Thirdly, the chemical structure–property relationships of A–D–A molecules will be highlighted. Next, we will focus on understanding why these A–D–A molecules show such outstanding device performance based on the fundamental mechanisms of OPVs. The device stability correlated to A–D–A molecules will also be commented on briefly. Lastly, an outlook and some suggestions will be given for improving A–D–A molecules in future studies in OPVs.

## 2. The structural and electronic characteristics of A–D–A molecules

The Donor–Acceptor (D–A) approach has been long used as an effective strategy for the design of high performance polymers

or small organic molecules in the organic electronics community, where “D” and “A” represent the electron rich and electron deficient moieties in the same molecule, respectively. Note that the above D/A terms have different meanings with regard to the donor and acceptor materials in the active layers in OPV devices. Unlike polymers generally featuring alternated D–A structures, there are many different D–A combinations for small molecules with defined structures, such as A–D–A, D–A–D, A1–D–A2–D–A1, D1–A–D2–A–D1, *etc.* However, the literature is still quite ambiguous in differentiating or defining these molecules clearly. Herein, in order to better see their intrinsic difference and find a way to define them, we have conducted a calculation analysis using the Gaussian16 method (see below for details) to evaluate the frontier electronic band structure and electron density distribution of different types of molecules. Then, the results from the calculation are used to directly correlate their frontier orbital charge density difference and the electron distributions in the excitation state to their structural features and photovoltaic performance.

Note that the well believed determining step for a high performance OPV device is the exciton charge separation, which intrinsically depends largely on the HOMO/LUMO electron density distribution and HOMO/LUMO levels of donor and acceptor molecules, since such a process happens in the excited state for both donor and acceptor molecules. It is probable that the interaction between the LUMOs of donor and acceptor molecules plays a major role, if not the most important one. With these considerations in mind, we first calculated the HOMO/LUMO for the two most important series of A–D–A and D–A–D molecules as shown in Fig. 2. If the excitation state is approximated as HOMO → LUMO electron transition, the charge density difference between the excited state and ground state of a given molecule can be evaluated as

$$\Delta Q = \Psi_{\text{LUMO}}^2 - \Psi_{\text{HOMO}}^2$$

The HOMO and LUMO calculations were carried out using the Gaussian16 method and optimized at the B3LYP/6-31G\* level, and the charge density difference ( $\Delta Q$ ) and integral calculations were conducted using the Multiwfn program.<sup>28</sup>

We then plotted the integral curves of the corresponding charge density difference  $\Delta Q$  along the longest axis of the defined molecules (black curves in Fig. 2). Meanwhile, in order to give an intuitive description of the charge density difference along the main backbone direction and for the convenience of discussion, the curves are simulated with low frequency wave functions by fast Fourier transform filters (red curves in Fig. 2). As shown in Fig. 2, the red fitted curves can be divided into different sections in terms of peak and valley, *i.e.* positive values for  $\Delta Q$  (peaks) should indicate that there is a larger electron density at the defined position (along the axis) on the LUMO compared with HOMO for this molecule, while a negative  $\Delta Q$  (valleys) indicates that there is a lesser electron density at the defined position on the LUMO. With these quantitative data, it is much easier and also we have a quantitative handle to see the intrinsic structural and electronic characteristics/features for most molecules. And more importantly, we can see

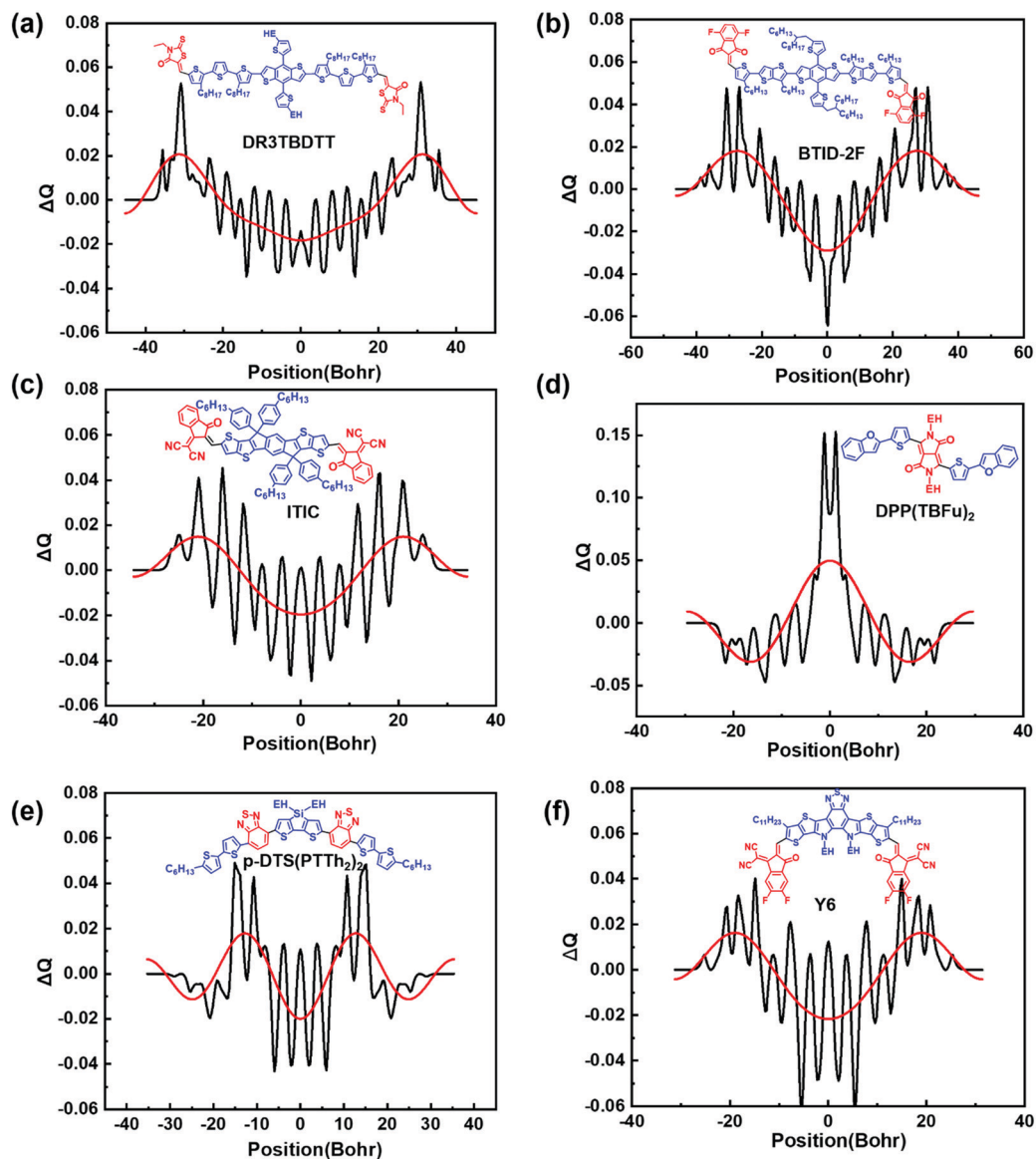


Fig. 2 HOMO/LUMO calculation and analysis of molecules with different architectures. Typical three A–D–A type molecules: donor (a) DR3TBDTT, donor (b) BTID-2F and acceptor (c) ITIC. One typical D–A–D type molecule: (d) DPP(TBFu)<sub>2</sub>. One typical D1–A–D2–A–D1 type molecule: (e) p-DTS(PTTh<sub>2</sub>)<sub>2</sub>. The current most successful acceptor molecule: (f) Y6. The black curves are the integral lines of the charge density difference ( $\Delta Q$ ) along the longest axis (backbone) of the defined molecules. The red curves are the simulated results with low frequency wave functions by fast Fourier transform filters.

the difference between various types of molecules, including some complicated molecules (such as Y6) which are not easy to define as A–D–A or D–A–D type molecules just based on the viewpoint of the A or D units. This advantage will be seen more clearly in later discussion. With this method, the well-performing donor molecules of DR3TBDTT<sup>29</sup> and BTID-2F<sup>19</sup> and the acceptor molecule ITIC,<sup>20</sup> each with only one clear A and D type section, all show the same peak–valley–peak plot along the molecule main backbone direction, and can be easily defined as A–D–A type molecules (Fig. 2a–c). In contrast, DPP(TBFu)<sub>2</sub><sup>26</sup> gives the shape of a valley–peak–valley plot (Fig. 2d), and thus could be defined as a D–A–D type molecule. As an example, for the case of the more complicated p-DTS(PTTh<sub>2</sub>)<sub>2</sub>

molecule with multiple A/D sections,<sup>27</sup> a more intricate curve of valley–peak–valley–peak–valley is obtained (Fig. 2e), corresponding to its D1–A–D2–A–D1 structure. However, its plot can still be arguably seen as a D–A–D type overall. Lastly, the current star molecule Y6 initially developed by Zou *et al.*,<sup>24</sup> from the viewpoint of its structural units, has multiple A/D sections. Its central unit (a benzothiadiazole unit with two side N atoms connected) is also hard to define as either an A or D unit. But based on the calculation shown in Fig. 2f, it has a typical peak–valley–peak plot curve, the same as those of DR3TBDTT, BTID-2F and ITIC molecules. With this, Y6 can thus be defined clearly as an A–D–A type molecule. Other OPV molecules with defined structures including donors and acceptors can be analysed in the same way and have similar results.

Due to the limit of space, these results will not be discussed here further, but the calculation results for some additional molecules have been given in the ESI.†

### 3. A brief history of A–D–A molecules

#### 3.1. A–D–A donor molecules

As discussed above, with the invention of PCBM based BHJ devices, studies in the OPV community turned to focus on looking for polymer donor materials with efficient absorption and matched energy levels with PCBM. Despite having a good film forming ability, polymers generally show the batch to batch variation issue in addition to their property-tuning problem. In contrast, small (oligomer) molecules exhibit advantages of essentially eliminated batch to batch issues due to their definite chemical structures and easily tuned properties. However, conventional organic molecules cannot form good films through solution processes and thus show much inferior photovoltaic device performance. This is why most small molecule based OPVs in the early stages were fabricated using the vacuum evaporation technique to form planar heterojunctions.<sup>15</sup> The situation was changed when solution processed A–D–A type donor small molecules were introduced by our group.<sup>17,30,31</sup> Prompted by the earlier small molecules for vacuum deposition OPVs,<sup>32,33</sup> we started with the design and synthesis of one dimensional oligothiophene derivatives with A–D–A architecture, in which a series of end groups with different electron withdrawing abilities were introduced; **1–8** are some representative ones (Fig. 3).<sup>17,30,31</sup> These A–D–A molecules were designed based on the following strategies. Firstly, the alkyl side chains and oligomer like backbones ensure those molecules to have a good film forming ability comparable to polymers. Secondly, it is equally important that using a conjugated oligomer backbone can achieve a similar light absorption efficiency as that of high performance polymers when the effective conjugation length is achieved. Thirdly, their absorption and energy levels can be tuned by both the end groups and central units since the LUMOs and HOMOs of those molecules are mainly determined by the end groups and central units, respectively. Lastly, the planar molecular backbones and conformation render those molecules to form effective/proper intermolecular packing and ensure them to show high mobility. Among them, the OPV device based on the 2:PC<sub>61</sub>BM blend film showed a high PCE of 6.10%, demonstrating the great potential of rhodanine based A–D–A molecules.<sup>30</sup> Following this, molecule **3** with 2-(1,1-dicyanomethylene) rhodanine as end groups showed an outstanding PCE of 9.30% with PCBM.<sup>31</sup> In addition to its efficient light absorption and other excellent features, the high device performance was also ascribed to the optimized morphology with an interpenetrating network consisting of ~10 nm diameter highly crystalline fibrils in its blending film with PC<sub>71</sub>BM, indicating that high device performances could be indeed realized by carefully tuning the chemical structure of molecules. Continuing on, a series of oligothiophene based molecules of DRCN4T-9T with different conjugation lengths, *i.e.* conjugated thiophene

numbers from 4 to 9, and spatial symmetry had been developed.<sup>18</sup> Among them, molecule **9** (DRCN5T) with five thiophene units in the backbone achieved a PCE of over 10% with the acceptor PCBM. In addition, it is worth noting that molecule **7** using the 1,1-dicyano methylene-3-indanone (INCN) unit,<sup>34</sup> the famous end group now widely used in current A–D–A acceptor molecules, exhibited a reduced bandgap and a wide absorption range extending to the near infrared range. However, molecule **7** has poor solubility in common solvents due to strong intermolecular interactions and could not form decent films for device evaluation. Fortunately, the solubility and overpacking issues could be overcome if INCN is combined with central building blocks having bulk steric units, as will be discussed in the next section. Later on, many other A–D–A small molecule donors have been designed following the above strategy.<sup>16</sup> Another representative series of A–D–A molecules are the benzo[1,2-*b*:4,5-*b'*]dithiophene (BDT) based A–D–A molecules,<sup>19,29,35,36</sup> in which the extended conjugated and planar backbones are formed after incorporating BDT as the central units. **10–13** in Fig. 3 are the typical molecules in this catalogue. With PCBM as the acceptor, molecules **10–13** all showed outstanding device performance with efficiencies around 10%.<sup>19,35,36</sup> Meanwhile, other building blocks such as porphyrin, dithienosilole units, *etc.* have also been introduced as central cores to design A–D–A donor molecules and showed promising device performances.<sup>16</sup> Recently, PCEs of over 13–14% have been achieved for A–D–A donor molecule based all-small-molecule devices.<sup>37,38</sup>

#### 3.2. A–D–A acceptor molecules

As an equal part to donors, acceptors have always played the same important role in the OPV devices with BHJ architecture. With isotropic electron transfer capabilities and high electron mobility, fullerene derivatives such as PC<sub>61</sub>BM and PC<sub>71</sub>BM had been the dominant electron acceptors since the invention of BHJ device structure in 1995.<sup>10</sup> However, the intrinsic properties of fullerene derivatives such as weak absorption and hardly tunable energy levels significantly limit their OPV performance. To address these issues, in the past few years, great attention has been given to non-fullerene acceptors (NFAs) in the OPV community. Various types of NFAs including small molecules and polymers have been designed and evaluated (Fig. 3).<sup>21</sup> With A–D–A structures same as the above donor molecules, molecules **14** and **15** are the first two typical ones used as acceptors,<sup>39,40</sup> but with limited PCEs of 2.43% and 3.08% with P3HT as the donor. But these promising results opened the avenue for A–D–A based acceptor design. The moderate push-pull interaction between the central D and the end rhodanine A unit of **15** contributes to its limited absorption and thus low current in the OPV devices. In contrast, an INCN unit has much stronger electron withdrawing ability and could also form strong intramolecular charge transfer (ICT) and afford significantly redshifted absorption. But molecules incorporating INCN would show poor solubility as in the case of donor molecule **7** if there is no bulk steric hindrance in the molecules. In 2015, an A–D–A acceptor **16**, namely ITIC, was reported by Zhan *et al.*, in which a fused core DTTDT was introduced as the

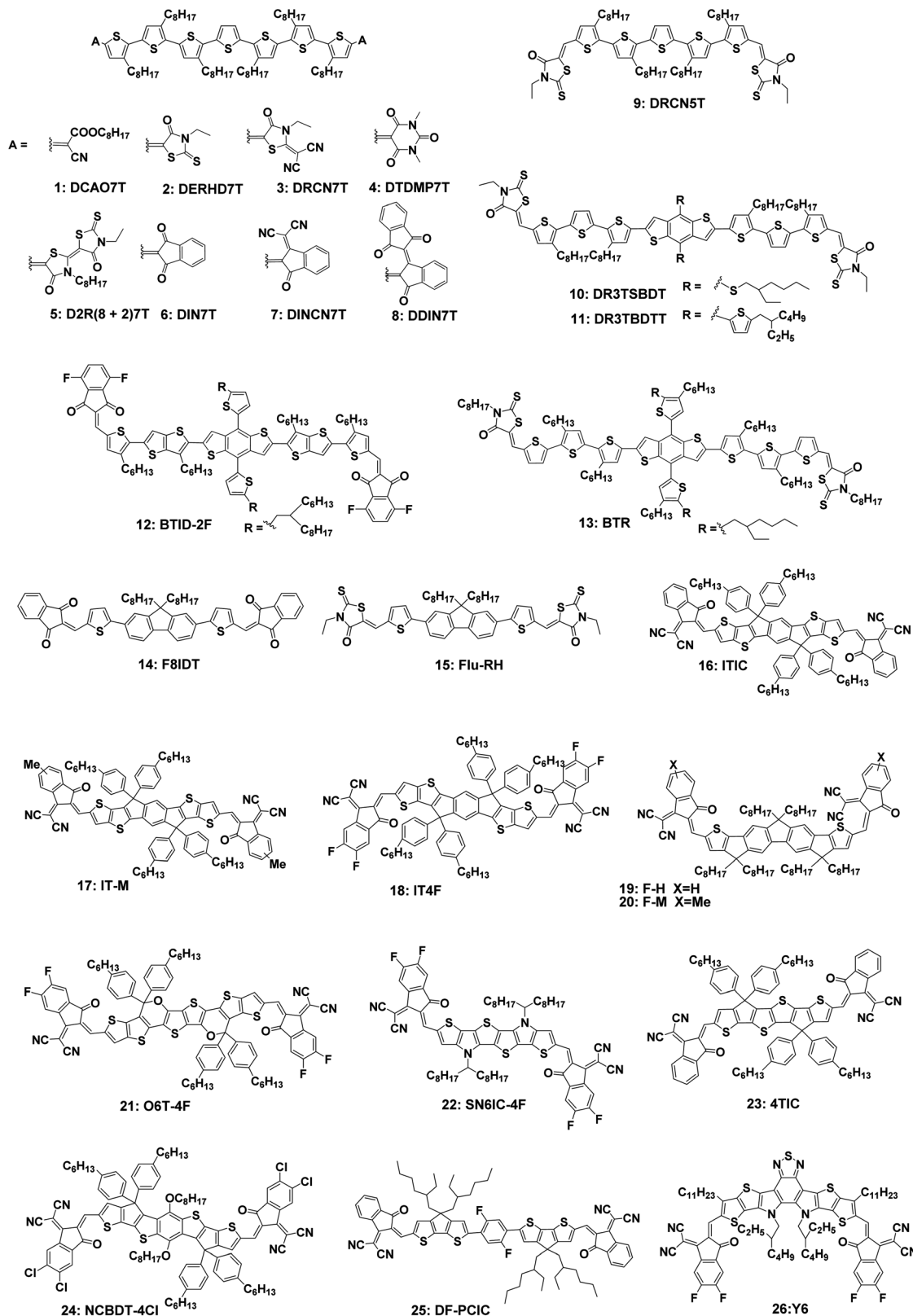


Fig. 3 Chemical structures of some typical A–D–A donor and acceptor molecules.

central D unit and INCN as the end group.<sup>20</sup> The fused central D unit DTTDT with bulk steric substitution prevents excessive

aggregation of the molecule and ensures good solubility of ITIC in common solvents and therefore an appropriate morphology

in the active layer blend. Thus, a promising PCE of 6.8% was achieved. Later on, following the same strategy, a series of acceptors with A–D–A structures have been designed through careful chemical modulation of ITIC, such as **17** (IT-M) and **18** (IT-4F) with record PCEs from 12% to 13%.<sup>41,42</sup> To date, many A–D–A type acceptors have been developed with various fused or unfused backbone D units, and most are with INCN or its derivatives as the end groups. Some typical A–D–A acceptors are shown in Fig. 3. Among them, with intrinsic A–D–A structures, acceptor **26** (Y6) and its derivatives have demonstrated outstanding device performance with PCEs of 15–17% for single junction devices.<sup>3,6,7,24</sup> With complementary absorption, A–D–A type acceptors **20** (F-M) and **21** (O6T-4F) were employed to fabricate tandem devices and a PCE of 17.3% was achieved.<sup>2</sup>

## 4. Chemical structure–molecular property relationship

It is important to note that absorption, energy levels, and packing of donor or acceptor molecules in the active layers all play vital roles in the overall OPV performance. Wide and strong absorption, matched energy levels between donor and acceptor, and molecular packing with suitable phase separation in the active layers are the most important prerequisites to achieve high efficiency. The A–D–A structure offers many advantages to finely tune/optimize those properties through dedicated molecular design and optimization.

### 4.1. Absorption

Organic materials whose absorption could be subtly tuned through molecular engineering indeed present an intriguing advantage. This is magnified in A–D–A molecules since their absorption can be effectively tailored by both the D and A moieties separately or combined together. Different absorption ranges of A–D–A molecules can be realized by changing the pull or push strength of A and D moieties due to the molecular orbital hybridization and ICT between D and A moieties. It is worth noting that A–D–A molecules in OPVs generally show a high extinction coefficient (around  $10^4$ – $10^5$  M<sup>-1</sup> cm<sup>-1</sup> at  $\lambda_{\text{max}}$ ) owing to the effective conjugated and planar molecular backbones.<sup>4,18</sup> Furthermore, higher absorption coefficient can be expected by enhancement of the HOMO–LUMO overlap through careful design of A–D–A molecules with delocalized molecular orbital density for HOMO and LUMO.<sup>43,44</sup> The long conjugated backbone can generally ensure efficient light absorption for the oligomer-like molecules. In addition, it is feasible to realize absorption tuning by varying individual components, especially the A unit, without changing the backbone structures, which brings great convenience and advantage for molecular design and synthesis. For instance, with the same backbone of septithiophene, molecules **1–8** showed different tunable absorption ranges owing to the different electron withdrawing abilities of the end groups (Fig. 4a). For ITIC derivatives, the absorption of ITIC to IT-4F redshifted from 700 to 717 nm with increasing electron withdrawing ability of

the end INCN groups.<sup>42</sup> Of course, the absorption can also be tuned by chemical modulation of the central D unit individually or collectively with the A unit. Introducing central D units with different electron donating ability and conjugation length and incorporating hetero atoms such as N and O on the backbones have all proved to be effective strategies to tailor the absorption of A–D–A molecules.<sup>45,46</sup>

On the other hand, the molecular packing behaviour in the solid state also plays an important role in the solid absorption, which is associated with molecular geometry structures such as planarity, conjugation length, side chains, *etc.* This is one of the eventual factors to determine the current of the devices. Most of the A–D–A molecules possess planar conjugated backbones, which is favourable for effective intermolecular packing/coupling and forming ICT in the solid state. For instance, with a planar conjugated backbone with a dihedral angle of  $0.3^\circ$  between the bridged thiophene and end groups, IEICO-4F exhibits an absorption onset up to 961 nm, which is 164 nm red shifted compared with that of its isomer molecule i-IEICO-4F. This is because i-IEICO-4F has a much twisted conjugated backbone with a dihedral angle of  $25.9^\circ$  between the bridged thiophene and end groups (Fig. 4b and c).<sup>47</sup> Bo *et al.* reported a molecular design strategy of noncovalent conformational locking to endow acceptor molecules with a good planarity in the solid state, which gave clearly red shifted absorption compared with the control molecule.<sup>48</sup> Besides the above factors, the side chains also have an effect on molecular absorption since the molecular packing is influenced by the side chains. An example is C8-ITIC, in which octyl chains were used to replace the hexylphenyl in ITIC. Compared with ITIC, C8-ITIC exhibits a reduction in the optical band gap with a red shifted absorption of 36 nm.<sup>49</sup> On the other hand, the low charge mobility of OPV materials leads to a limit on the active layer thickness and efficient light absorption. More efficient sunlight can be absorbed and favour for improving OPV device current if active layer material has high mobility and thus its thickness could be increased. To this end, if the backbone D units and the end group A units can simultaneously form intense interactions through careful design of molecules, high mobility as well as efficient absorption could be expected, which should be a feasible pathway for further improving device photocurrent from the viewpoint of absorption.

### 4.2. Molecular orbital energy levels

State-of-the-art OPV devices have a BHJ active layer, in which donor and acceptor materials are mixed to form an interpenetrating morphology. This requires that the donor and acceptor materials have matched energy levels to facilitate exciton separation and charge transfer. In addition, the photovoltaic parameter  $V_{\text{oc}}$  is tightly correlated with the energy level difference between the HOMO of the donor molecule and the LUMO of the acceptor molecule. Thus, molecular orbital energy level control is one of the key points in OPV molecule design.

With the hybridization of frontier orbitals between D and A units, the HOMO and LUMO of an A–D–A molecule are primarily determined by its central D and end A units, respectively.

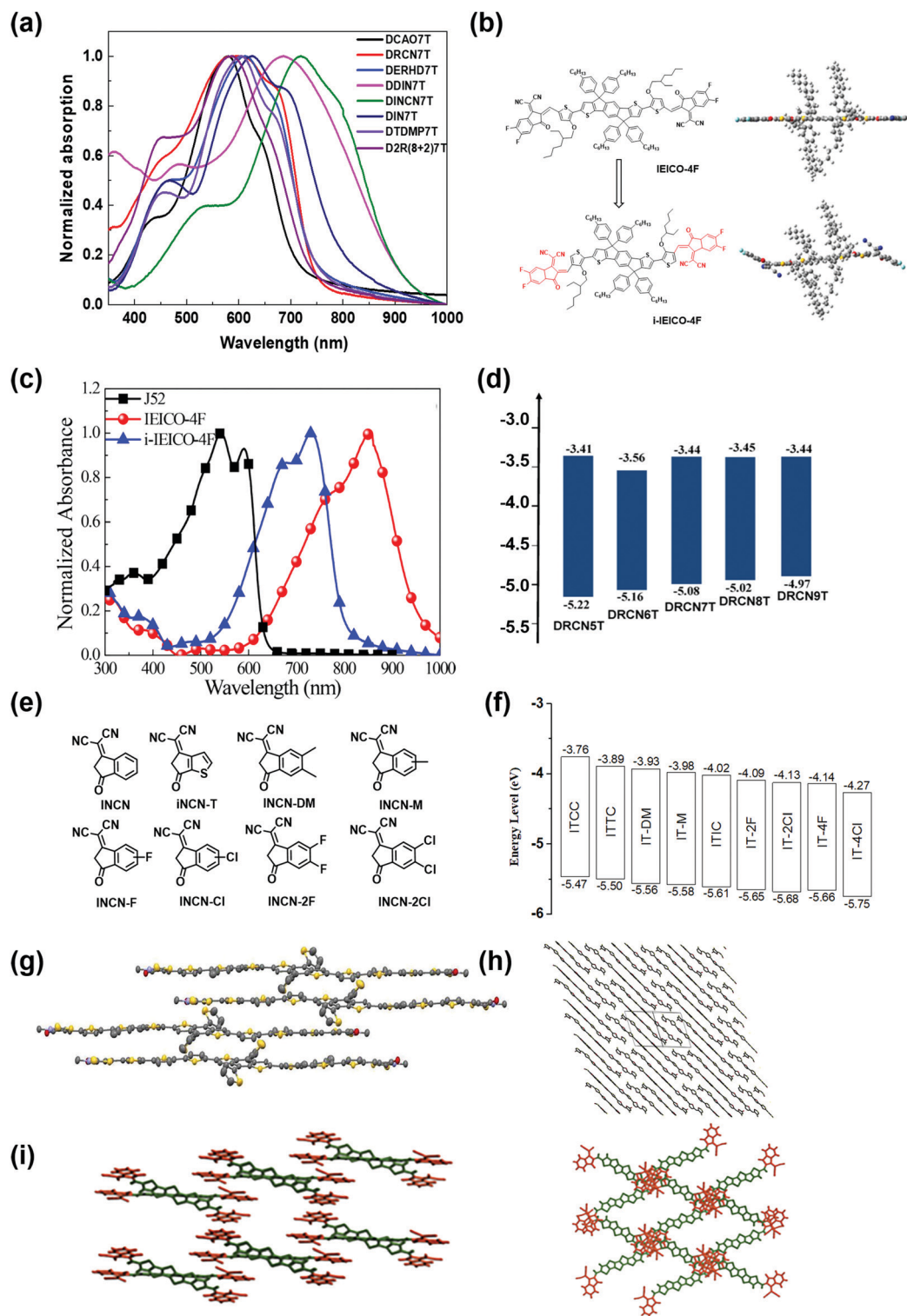


**Fig. 4** Absorption, energy levels, and packing of some typical A-D-A molecules. (a) The absorption spectra of A-D-A molecules **1–8** with a septithiophene backbone. (b) Chemical structures and simulated molecular geometries and (c) absorption of IEICO-4F and i-IEICO-4F. (d) Energy levels of DRCN4T-5T small molecules. (e) Chemical structures of the typical INCN unit and its derivatives. (f) Energy levels of ITIC and its derivatives with INCN derivatives as end groups. (g) Side view of BTR aggregation. (h) Crystal packing of BTR backbones. The  $\pi$ -stacking extends in a brick-wall type pattern within the crystallographic (011) plane. (i) Crystal packing of 4TIC, in which the side chains of hexylphenyl groups are omitted for clarity. There exists close  $\pi$ - $\pi$  stacking between the terminal acceptor INCN units, while there is no intermolecular interaction such as  $\pi$  stacking found between the center cores owing to the bulky hexylphenyl groups. Reprinted with permission from ref. 47 (b and c, copyright 2018 American Chemical Society), ref. 18 (d, copyright 2015 American Chemical Society), ref. 36 (g and h, copyright 2015 Nature Publishing Group) and ref. 57 (i, copyright 2017 American Chemical Society).

Thus, one can tune the HOMO and LUMO of an A–D–A molecule through optimization of D and A units separately/combined. The LUMO will shift down with the increasing electron-withdrawing ability of the A unit, and the HOMO will shift up with the increasing electron-donating ability of the D unit. For instance, the LUMO levels decreased when increasing the strength of A end groups in the septithiophene series of molecules, while the change in HOMO was minor.<sup>34</sup> In the DRCN5T–9T series of molecules with the same end groups, the HOMOs increased from  $-5.34$  eV of DRCN4T to  $-4.97$  eV of DRCN9T with increasing conjugation length and their LUMOs remained nearly unchanged with values around  $3.40$  eV (Fig. 4d).<sup>18</sup>

The LUMOs of A–D–A type molecules can be most effectively tuned through their two electron deficient end groups, which render them some advantages as acceptor materials compared with other types of molecules. With unique chemical structures and suitable energy levels, INCN and its derivatives (Fig. 4e) stand out to be the best and most commonly used end groups in the A–D–A acceptor molecule design, and indeed have been used in most high performance acceptor molecules. The energy levels of A–D–A molecules could be efficiently tailored by using different INCN derivatives with different electron withdrawing abilities (Fig. 4e and f). Noticeably, those A–D–A acceptors incorporating INCN and its derivatives showed LUMOs around  $4.0$  eV, which is a value comparable to that of PCBM. This means that the large library of existing donor materials with energy levels matched with PCBM could be used directly without worrying about the energy level matching issue. On the other hand, the large and planar structure of INCN and its derivatives helps to form effective intermolecular  $\pi$ – $\pi$  interactions between the acceptor molecules in the solid state, which could facilitate efficient charge transport. This will be addressed more in the next section.

#### 4.3. Molecular packing

For the molecular properties discussed above, molecular packing in the active layer has a crucial influence on the active layer's morphology and electronic processes for OPVs, and thus is another critical factor impacting the overall OPV performance. Current studies in this area lack insight at the molecular level and need much more focus in the future. Most A–D–A molecules have a planar molecular backbone with side chains of different lengths and orientations. Thus, the packing modes of A–D–A molecules are mainly determined by the molecule's overall configuration and end groups, which can be seen from the reported single crystal X-ray results of A–D–A molecules.<sup>33,36,50</sup> For example, the molecule BTR (13) has a coplanar structure of the conjugated backbone without bulk hindrance side chains, which renders its crystal stacking through the backbone  $\pi$ – $\pi$  interaction.<sup>36</sup> As shown in Fig. 4g and h,  $\pi$ -stacked centrosymmetric dimers are formed with an average interplanar separation of *ca.*  $3.60$  Å, which further aggregate together by  $\pi$ -stacking with an average interplanar separation of  $3.62$  Å and form a brick-wall type pattern. The planar conjugated backbone facilitates the above crystal stacking, which leads to the ordered packing behaviour in the active layer. This type of packing has also been found in other A–D–A donor

molecules such as DCV5T–Me with a five thiophene unit backbone.<sup>33</sup> While single crystal X-ray results of most other A–D–A donor molecules have not been obtained, it is believed that they should have a similar packing mode in the solid state. This should be one reason for their high performance as donors.

However, the packing mode is different for the most current A–D–A acceptor molecules because of their fused center core units and their rather bulky side chains. In the reported A–D–A acceptor crystals, *e.g.* 4TIC,<sup>50</sup> the molecular backbones are essentially planar, with the hexylphenyl groups oriented outward. Importantly, no intermolecular  $\pi$  stacking is found between the molecular backbone D units owing to the large hindrance of bulky hexylphenyl groups. Furthermore, although their exact packing modes are different, there clearly always exists close  $\pi$ – $\pi$  stacking between the INCN end groups in those A–D–A acceptor crystals (*e.g.* 4TIC in Fig. 4i). In other words, the solid packing behaviours of these molecules are mainly determined by the end-group  $\pi$ – $\pi$  interaction. It is worth noting that the strong interaction between the end groups should contribute to form excellent isotropic electron transport channels among A–D–A molecules in their domains in the active layer.<sup>51</sup> This may be one of the main reasons why these acceptor molecules with an A–D–A structure show outstanding properties and device performance. It is believed that better and properly ordered packing could be achieved if the backbone D units could simultaneously form intense interactions through careful molecular design, as seen in the A–D–A donor molecules discussed in the last section, and that this should further facilitate charge separation/transportation.

## 5. Why do A–D–A molecules show excellent performance?

It is undoubted that so far A–D–A molecules have demonstrated great success in contrast to other types of OPV molecules with defined structures. This raises the long-sought question, *i.e.* why do A–D–A type molecules show such good performance? Note that most typical OPV molecules with defined structures belong to A–D–A and D–A–D types as discussed in the previous section. Both types of these molecules should essentially have the same capability to tune their structures/units to have optimal absorption, energy level, molecular packing, *etc.*, as discussed above. So there must be some other clear difference between these two types of molecules, which should be the main cause for their performance difference. Thus, in the following section, using the clear structural and electronic difference presented above, we will discuss and propose our understanding why A–D–A type molecules have higher OPV performance in general.

### 5.1. The photovoltaic mechanism behind A–D–A molecule based devices

For the photovoltaic process in an organic photovoltaic device, there are four major steps in the accepted mechanism: (1) photon absorption and exciton generation, (2) exciton diffusion, (3) exciton dissociation and charge separation, and (4) charge transport and collection (Fig. 5a). In the above four steps, the

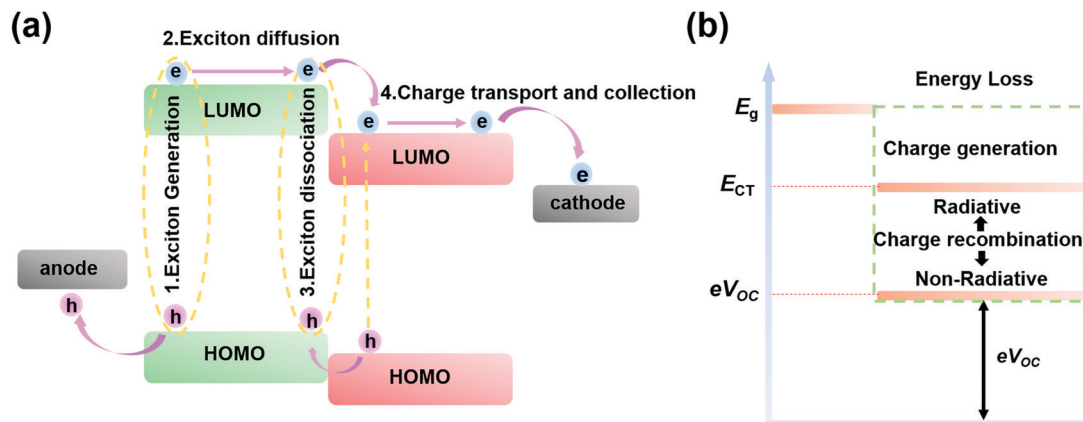


Fig. 5 (a) Diagram of the working mechanism of OPVs. (1) Photoexcitation to generate an exciton. (2) Exciton diffusion to the donor–acceptor interface. (3) Exciton dissociation at the donor–acceptor interface. (4) Free charge carrier transport and collection at the external electrodes. (b) The  $E_{loss}$  from  $E_g$  to  $eV_{oc}$ .  $E_{loss}$  for OPVs can be separated as that which is incurred during charge generation ( $E_g - E_{CT}$ ) and that which is incurred during charge recombination ( $E_{CT} - eV_{oc}$ ). Charge recombination energy loss results from both radiative and non-radiative CT state decay.

3rd step is a critical one,<sup>52</sup> where highly efficient exciton dissociation and charge separation with no charge recombination is highly desirable and decides largely the EQE ( $J_{sc}$ ) and FF. The interaction between donor and acceptor molecules in the active layer plays a great role, if not the most important one, in the 3rd step.<sup>53</sup> Such interaction should mainly depend on the LUMO orbitals/interaction of the donor and acceptor, as the exciton dissociation and charge separation step 3 happens in the excited state for both donor and acceptor molecules. Thus, proper interaction between such two LUMO orbitals should favour an efficient charge separation. As shown in Fig. 2, A–D–A molecules show larger electron density distribution (Fig. 2a–c and f) in LUMOs in the two end group parts for both donor and acceptor types of molecules, such as DR3TSBDT, ITIC, Y6, *etc.* This would, in the donor/acceptor blend, facilitate the exciton dissociation process (charge separation) at the D/A interface owing to the strong interaction/coupling between the LUMOs of donors and acceptors. With this, A–D–A molecules should show advantages in maximizing exciton dissociation. And as a competitive process, the charge recombination (geminate recombination) can be reduced.<sup>54</sup> On the other hand, the D–A–D type molecules, such as DPP(TBFu)<sub>2</sub>, have larger electron density distribution (Fig. 2d) in the middle part of the molecule. This would put some hindrance in the LUMO interaction of the donor and acceptor molecules, at least from the viewpoint of space access. Yi *et al.* have investigated the impact of small molecule donors with different architectures on interfacial arrangements and intermolecular charge-transfer processes by means of multiscale theoretical simulations.<sup>55</sup> They have found that for A–D–A type molecules, such as DR3TBDTT, DR3TBDT, and DR3TSBDT, the molecular architecture benefits exciton dissociation and the charge separation process and also suppresses charge recombination, in contrast to D–A–D type molecules. They proposed that such benefits should come from the large electron distribution of LUMO and LUMO+1 at the end sides (A units), mainly caused by the rhodanine end group. Furthermore, owing to the hindrance of the central D unit in these molecules, the acceptor PC<sub>71</sub>BM

molecule can come into close contact with the two electron deficient end groups of those A–D–A molecules, which facilitates exciton dissociation and reduces charge recombination simultaneously; this cannot be realized in molecules with other types of structures such as D–A–D molecules.

For acceptor molecules, currently the most successful small molecules with defined structures include ITIC, F-M and Y6 molecules. Note that these molecules all have bulk hindrance in the molecular backbone but with planar end units such as INCN. As shown in Fig. 2, these molecules all have a peak-valley-peak curve for the electron density distribution. Thus, they tend to form three dimensional molecular packing through intermolecular  $\pi$ - $\pi$  stacking between the planar end INCN groups or INCN derivatives, which has been confirmed by single crystal X-ray results.<sup>50,56</sup> Thus, similar LUMO strong interactions as that for the case of A–D–A type donor molecules discussed above could exist. This should facilitate charge separation in the key exciton dissociation step. Furthermore, such strong LUMO coupling between the neighbouring molecules in each of the donor and acceptor domains should generate three-dimensional charge transportation channels respectively for both electrons and holes. Indeed, efficient isotropic electron mobility and transport along three dimensions have been observed.<sup>56</sup> Also, Wei *et al.* reported recently that such three-dimensional molecular packing of A–D–A acceptor crystals could lead to low exciton binding energy ( $E_b$ ).<sup>57</sup> The  $E_b$  values calculated in solid crystals by a self-consistent quantum mechanics/embedded charge method could be as small as 0.16 eV for 6TIC-4F and even 0.04 eV for 4TIC, which are comparable to that of perovskites. These results imply that exciton generation in OPVs might be realized by only thermal energy without any extra driving force using A–D–A molecules, further indicating the advantages of A–D–A type molecules for OPVs.

In short, the two most important steps in the OPV mechanism, exciton separation and charge transportation, are both facilitated in A–D–A type molecules, due to their favourable frontier electron density distribution with higher density at the outside ends compared with other molecule types such as D–A–D.

## 5.2. Energy loss of A–D–A molecule based devices

Organic photovoltaic cells generally show large energy losses ( $E_{\text{loss}}$ ) compared with crystalline silicon or perovskite solar cells, which is due to the large exciton binding energy and charge recombination in organic semiconductor films. As shown in Fig. 5b,  $E_{\text{loss}}$  is defined as  $E_{\text{loss}} = E_g - eV_{\text{oc}}$ , where  $E_g$  is the smaller optical bandgap of donor or acceptor. In order to overcome the binding energy of excitons, an active layer incorporating donor and acceptor with energy offset is required to provide the electron–hole separation driving force ( $E_g - E_{\text{CT}}$ ). Charge recombination ( $E_{\text{CT}} - eV_{\text{oc}}$ ) can be divided into radiative and non-radiative recombination. Radiative recombination is inevitable and intrinsic for all systems. Thus, non-radiative recombination is another source of  $E_{\text{loss}}$  and should be focused on for optimized OPVs.<sup>58</sup>

Although much progress has been made for the A–D–A based OPVs with low  $E_{\text{loss}}$  through molecular design and device optimization, the detailed mechanism behind its success is complicated and remains unclear. Additionally, it is still a considerable challenge for OPVs to achieve  $E_{\text{loss}}$  comparable to that of inorganic solar cells. However, it is exciting to see that recent results from A–D–A acceptor based devices are very promising and show their great potential in reducing  $E_{\text{loss}}$ .<sup>59</sup> Considering the large electron density distribution on the two end groups (Fig. 2), A–D–A molecules exhibit the advantage of having efficient charge separation, owing to the strong coupling of the LUMOs of donor and acceptor molecules at the interface, and have the potential to greatly reduce charge generation incurred  $E_{\text{loss}}$ .

A great number of A–D–A based devices have now demonstrated small  $E_{\text{loss}}$  values below 0.6 eV,<sup>21</sup> which are much lower than those of fullerene based devices. For instance, Jen *et al.* reported a dithienopicenocarbazole based A–D–A acceptor DTPC-DFIC and its device based on PTB-Th:DTPC-DFIC showed an extremely low  $E_{\text{loss}}$  of 0.45 eV with a high PCE of 10.21%.<sup>60</sup> After careful investigation of a series of A–D–A acceptor based devices, Gao *et al.* have found that a low energy offset between donor and acceptor materials in the blend would be favourable to have small  $E_{\text{loss}}$ . This could be indicated by a high photoluminescence yield of the active material.<sup>59</sup> The results are consistent with recent reports from McCulloch's group.<sup>61</sup> They reported two A–D–A acceptor FBR and IDTBR based devices with high  $V_{\text{oc}}$  of 1.12 and 1.07 V and  $E_{\text{loss}}$  of 0.5 and 0.55 eV, respectively. It was found that the two devices showed small energy offsets (0.05 and 0.2 eV) with higher  $\text{EQE}_{\text{EL}}$  values ( $10^{-3}$ ) than the control device with PC<sub>71</sub>BM as the acceptor ( $V_{\text{oc}}$  0.76 V, energy offset 0.4 eV and  $\text{EQE}_{\text{EL}}$   $10^{-4}$ ).

These results indicate that A–D–A type molecules could not only have better exciton separation and charge transportation, but could also have a smaller  $E_{\text{loss}}$ .

## 6. A–D–A molecules for high stability OPV devices

Stability is a critical factor as important as efficiency for future commercial applications of OPVs. There are many complicated external and intrinsic factors that affect stability. Thus, only a very brief discussion will be presented here. The extrinsic

factors such as oxygen and water can be avoided in principle through careful encapsulation. The intrinsic factors depend on the chemical structures of the materials, especially the ones in active layers. The commercial application of organic light emitting diodes (OLED) proves that the intrinsic chemical stability of active materials might not be a problem for active layer materials in OPVs if the same strategy applied for OLED materials is used in OPVs. Another side of intrinsic stability for OPVs is the morphological stability of the active layer.<sup>62</sup> In the state-of-the-art OPV devices with BHJ structure, the donor and acceptor are mixed to form composite morphology with nanometer scale separated donor/acceptor regions to facilitate exciton dissociation and charge transport. It is well known that the active layer morphology can be carefully optimized to ensure an appropriate phase separation to maximize the efficient exciton separation and charge transportation for high performance devices.<sup>52</sup> However, both the donor and acceptor molecules in the optimized active layer can still migrate and rearrange into a thermodynamic equilibrium (or more stable) state during the path of long-time utilization, since the morphological state of the initial active layer might not be a thermodynamically stable state. Note that this morphological change will still happen even if the initial state has optimal morphology for high power conversion. In other words, the morphological metastability would lead to the degradation of device performance over time. For example, many fullerene based BHJ devices show a significant initial loss of performance referred to as “burn-in” loss, which mainly comes from morphological instability owing to fullerene aggregation or demixing with donor materials.<sup>63</sup>

As various A–D–A molecules have been designed and they also afforded high efficiencies refreshed frequently, stability becomes increasingly vital for the coming commercialization of OPVs. With their unique chemical and electronic structures, A–D–A molecules also show great potential for high stability devices. Firstly, A–D–A molecules generally show good chemical stability and are not sensitive to oxygen or water. Secondly, and maybe most importantly, A–D–A molecules are easy to pack closely due to the strong interaction between the strong end groups such as INCN, which might render them form a stable phase/morphology in the active layers. Thus, A–D–A molecules tend to form a stable morphology and would help to improve device stability. For example, a burn-in free device was reported by Gasparini *et al.* using an A–D–A acceptor IDTBR with P3HT as the donor.<sup>64</sup> There was only 5% loss of PCE for the P3HT:IDTBR device under light-soaked conditions over 2000 h (Fig. 6a). In contrast, the control device with PCBM showed a loss of ~34% in hundreds of hours. The better stability of A–D–A molecule IDTBR based devices has been proposed to stem from the well stable morphology of the active layer with unchanged crystallinity of the acceptor and donor, while fullerene tended to mix into P3HT to decrease the crystallinity of the polymer phase. Recently, Li *et al.* reported the photo-stability of the devices of A–D–A type acceptor ITIC and its four derivatives.<sup>65</sup> Devices based on ITIC-2F (also named IT-4F) and ITIC-Th showed a T80 lifetime (80% of the initial PCE) of over

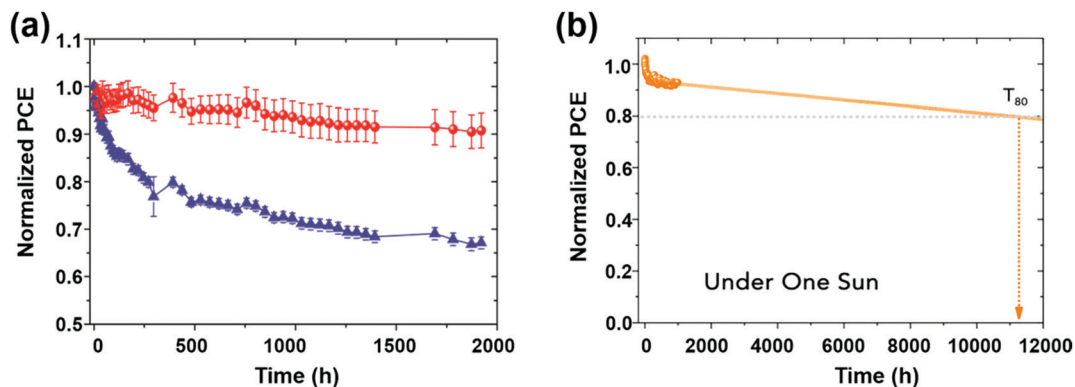


Fig. 6 (a) Normalized PCE of P3HT:IDTBR and P3HT:PCBM solar cells in the course of 2000 h of light exposure. (b) PBDB-T:ITIC-2F based devices show extrapolated operational lifetime approaching 10 years. Reproduced with permission from ref. 64 and 65 (copyright 2017 Wiley-VCH and 2019 Cell Press).

11 000 h, approaching 10 years of operational lifetime (Fig. 6b). It should also be noted that ITIC, ITIC-M and ITIC-DM based devices showed inferior stability. Additionally, ITIC-DM based devices showed strong burn-in losses of  $J_{sc}$  and FF owing to the chemical and morphological instability of ITIC-DM. The 10 year lifetime of PBDB-T:ITIC-2F based devices is an exciting result for OPVs. The direct correlation of device stability and A-D-A molecules' chemical structures has thus given both opportunity and challenges for chemists to design molecules for devices with both high efficiency and stability.

## 7. Summary and outlook

Despite the success of A-D-A molecules, much work is still needed to be done for the future application of OPVs, including achieving higher PCEs, longer time stability, and addressing process issues for large scale production. Among them, higher PCEs are still strongly desirable for OPV commercialization, which is indeed the priority consideration for all PVs, including crystal silicon and perovskite solar cells. Better active layer materials are still believed to be the main driving force to address all of the above issues. The present success of A-D-A molecules will definitely give very valuable insights into designing better active layer materials, especially new A-D-A molecules with higher performance. We strongly believe that improved molecules with A-D-A structures that demonstrate higher performance and meet the requirements of OPV commercialization will emerge soon in the near future.

For future design of better OPV molecules, we think some general rules and guidelines presented below may prove helpful. (1) The molecules should have the intrinsic frontier electron density distribution of A-D-A type molecules, *i.e.* exhibit a similar  $\Delta Q$  curve shape of peak-valley-peak as that of the typical A-D-A molecules in Fig. 2a-c and f, favouring the two important steps (exciton separation and charge transportation) in the OPV mechanism. (2) In addition to the consideration of solubility and over-aggregation issues, molecules with enhanced/proper  $\pi$  intermolecular interaction among both A end units and backbone might be helpful to give higher mobility and relatively improved

light absorption in the solid state. This could make these devices perform better than those based on the molecules with the same molecular level properties. (3) It is suggested to use the semi-empirical model analysis, as discussed below, for the absorption range and energy level values for both single-junction and tandem cells. Keeping these general considerations in mind, further detailed discussions are presented below.

### 7.1. Better understanding of the correlation between chemical structure and property

With the unique structural and electronic features discussed above, in addition to the general advantages such as easy and effective tuning of absorption, energy levels and even packing modes, A-D-A type molecules exhibit some superior intrinsic properties favouring the photovoltaic process such as efficient exciton dissociation and charge transport, and low voltage loss. To date, many A-D-A molecules have been designed from the perspective of optimization of the core units, spacers, side chains and end groups and afford outstanding device performance. However, the underlying relationship and mechanism between the molecular chemical structures and properties still need to be investigated thoroughly to design better molecules with higher device performance. For example, it should be noted that the absorption of star molecule Y6 redshifts about 100 nm from solution to solid film,<sup>24</sup> which is larger than the difference for most of the A-D-A molecules. This should cause better molecular packing and more appropriate morphology in the active layer, leading to its superior performance. Unlike conventional and most A-D-A acceptors with only interactions between the end groups, there might exist interactions between the backbones too. This may be the main reason why this molecule exhibits much better performance than most current acceptor molecules. With this, it would be a good strategy to design OPV molecules with effective interactions/packing with both end groups and backbones.

### 7.2. Molecular design for higher device efficiency

Based on the semi-empirical analysis that we previously reported, the predicted PCEs could be over 20% for single-junction OPVs (Fig. 7a).<sup>2</sup> As shown in Fig. 7a, if a single junction device has an

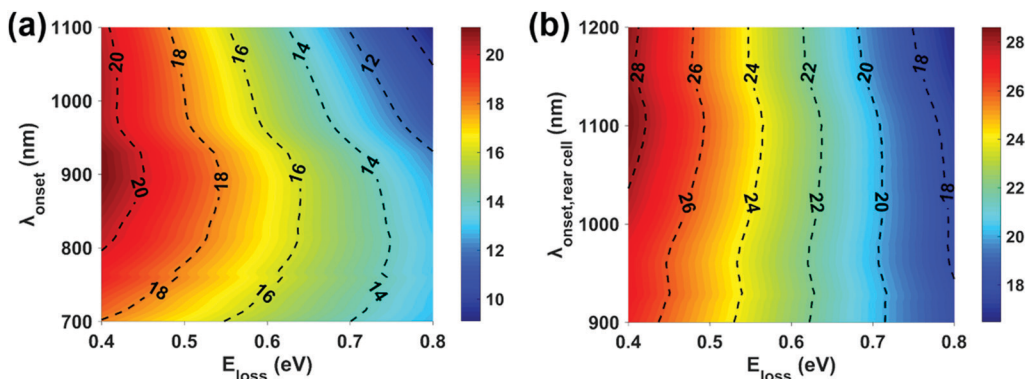


Fig. 7 Predicted PCEs vs.  $E_{\text{loss}}$  and active layer absorption onset  $\lambda$  with an assumed average EQE of 80% and an FF of 0.80 for single junction (a) and two terminal tandem (b) OPVs based on a semi-empirical analysis.

absorption onset around 900–1100 nm and average EQE response 80%,  $E_{\text{loss}}$  below 0.45 eV and FF 80%, a high efficiency of 20% could be reached. In fact, each of the above parameters has been achieved separately. The challenge is to achieve them altogether in one device through delicate active layer molecule design and device optimization. Note that Y6 and its derivatives reported to date have shown promising PCEs of 16–18%.<sup>3–7</sup> But their devices show  $V_{\text{oc}}$  around 0.82–0.86 V with  $E_{\text{loss}}$  over 0.47 eV,  $J_{\text{sc}}$  26–28  $\text{mA cm}^{-2}$  with an absorption onset of 930 nm and average EQE below 80%, and FF around 77%. Clearly, compared with the modelling shown in Fig. 7a, there is still much room for improvement for each of these parameters. Thus, the overall performance still has large room to grow. For the state-of-the-art high efficiency BHJ devices, the donor and acceptor each absorbs light in the short and long wavelength region respectively. Thus, the absorption onset of the active layer is determined by the acceptor and  $\lambda_{\text{onset}}$  in Fig. 7a is also the absorption onset of the acceptor. With this, the absorption onset of the acceptor should be first considered to ensure higher  $J_{\text{sc}}$  with a range of around 950 nm (note that the absorption onset of Y6 is 930 nm) for high performance single junction devices. Meanwhile, the donor should be designed or selected with an acceptor with the matched efficient absorption and energy level. On the other hand, designing the donor and acceptor to have a low energy offset and high luminescence is preferred to have low  $E_{\text{loss}}$  and high  $V_{\text{oc}}$ .<sup>59</sup> And the high and balanced mobility of electrons and holes in the blending film could give a high FF, which might be achieved by designing some molecules with better packing, such as three dimensional packing. If all of the above optimizations could be achieved, with an acceptor absorption onset of around 950 nm ( $J_{\text{sc}}$  is 28.56  $\text{mA cm}^{-2}$  with average EQE 80%),  $V_{\text{oc}}$  0.9 V ( $E_{\text{loss}}$  0.4 eV) and FF 80%, a PCE of 20.56% could be expected for a single junction device.

Tandem cells could address the issues of limited sunlight absorption and the thermalization loss of photon energy, and arguably it might be best to use OPVs for tandem cells.<sup>2</sup> For the widely studied 2-terminal (2T) monolithic tandem cells, the overall  $V_{\text{oc}}$  is the sum of  $V_{\text{oc}}$  values of the subcells, and  $J_{\text{sc}}$  is generally limited by the subcell with the smallest one. Following the semi-empirical model analysis (Fig. 7b), PCEs >28% are

predicted for 2T tandem cells.<sup>2</sup> Presently, for high performance 2T tandem cells, there have been some decent choices of materials with suitable absorption and device performance for the front subcell. So the first thing is to have suitable rear subcell active materials with an infrared absorption onset up to 1050–1150 nm from the results shown in Fig. 7b. Meanwhile, the performance of these rear cell materials should also have low  $E_{\text{loss}}$ , optimal FF and EQE, *etc.* in their single junction cell evaluation. However, the presently reported active layer molecules cannot meet these requirements yet. Thus, acceptor molecules with infrared absorption with an onset up to 1050–1150 nm should be urgently designed for high performance tandem cells since the absorption onsets of nearly all the current high performance OPVs are determined by the acceptors. To have possibly maximized matched  $J_{\text{sc}}$  with the rear cell, the front cell should have complementary absorption with an onset of around 720 nm. Meanwhile, the two subcells should have minor  $E_{\text{loss}}$  to have high  $V_{\text{oc}}$  and thus ensure high  $V_{\text{oc}}$  for the tandem devices. This could be done by following the same design strategy of active layer molecules for single junction devices. In addition, the interconnection layer materials should form an effective Ohmic contact and charge extraction and recombination between the front and rear cells.<sup>2</sup> Assuming a  $E_{\text{loss}}$  of 0.4 eV, an average EQE of 80% and a FF of 80%, and absorption onsets of 1100 nm and 720 nm for the rear and front cells, respectively, a PCE of 28.60% can be obtained for a 2T tandem device.

It is worth noting that donor molecules indeed play a critical role similar to that of acceptors. Presently, most high performance OPVs are fabricated using A–D–A molecule acceptors and polymer donors.<sup>25</sup> In contrast, relatively less progress has been observed recently regarding donors. Considering the well-known batch-to-batch variation issue for polymers, much effort should be devoted to small molecular type donors such as A–D–A type molecules, including importantly for the all small molecular type devices.<sup>37,38</sup> Considering the success of A–D–A donor molecule based devices with PCBM, and the advantages of A–D–A molecules discussed above, OPVs based on all A–D–A molecules, *i.e.* A–D–A donor and acceptor devices, are strongly believed to have an exciting opportunity offering comparable and perhaps even better performance compared with the

corresponding polymer donor based devices. In this regard, a recent case has demonstrated such potential with a PCE of over 14% for an all-small-molecule device.<sup>38</sup> For the design of A–D–A donor molecules in all small molecule devices, besides the conventional considerations such as complementary absorption and matched energy levels with acceptors, the miscibility with the A–D–A acceptor should be particularly addressed. This is because the morphological control with suitable phase separation in all small molecule active layers seems to be a challenge owing to the similar chemical and electronic structures of A–D–A donor and acceptor. Thus, using the modelling results presented above as a guideline, synergistic design of A–D–A donor and acceptor in terms of all the factors discussed above is strongly suggested.

## Conflicts of interest

There are no conflicts to declare.

## Acknowledgements

The authors gratefully acknowledge the financial support from MoST (2016YFA0200200 and 2019YFA0705900) and NSFC (21935007 and 51773095) of China, Tianjin city (17JCJQC44500) and 111 Project (B12015).

## Notes and references

- 1 A. J. Heeger, *Adv. Mater.*, 2014, **26**, 10–27.
- 2 L. Meng, Y. Zhang, X. Wan, C. Li, X. Zhang, Y. Wang, X. Ke, Z. Xiao, L. Ding, R. Xia, H.-L. Yip, Y. Cao and Y. Chen, *Science*, 2018, **361**, 1094–1098.
- 3 Y. Lin, B. Adilbekova, Y. Firdaus, E. Yengel, H. Faber, M. Sajjad, X. Zheng, E. Yarali, A. Seitkhan, O. M. Bakr, A. El-Labban, U. Schwingenschlogl, V. Tung, I. McCulloch, F. Laquai and T. D. Anthopoulos, *Adv. Mater.*, 2019, **31**, 1902965.
- 4 Y. Cui, H. Yao, J. Zhang, T. Zhang, Y. Wang, L. Hong, K. Xian, B. Xu, S. Zhang, J. Peng, Z. Wei, F. Gao and J. Hou, *Nat. Commun.*, 2019, **10**, 2515.
- 5 Q. Liu, Y. Jiang, K. Jin, J. Qin, J. Xu, W. Li, J. Xiong, J. Liu, Z. Xiao, K. Sun, S. Yang, X. Zhang and L. Ding, *Sci. Bull.*, 2020, **65**, 272–275.
- 6 K. Jiang, Q. Wei, J. Y. L. Lai, Z. Peng, H. K. Kim, J. Yuan, L. Ye, H. Ade, Y. Zou and H. Yan, *Joule*, 2019, **3**, 3020–3033.
- 7 B. Fan, D. Zhang, D. Li, W. Zhong, Z. Zeng, L. Ying, F. Huang and Y. Cao, *Sci. China: Chem.*, 2019, **62**, 746–752.
- 8 C. W. Tang, *Appl. Phys. Lett.*, 1986, **48**, 183–185.
- 9 J. C. Hummelen, B. W. Knight, F. Lepeq, F. Wudl, J. Yao and C. L. Wilkins, *J. Org. Chem.*, 1995, **60**, 532–538.
- 10 G. Yu, J. Gao, J. C. Hummelen, F. Wudl and A. J. Heeger, *Science*, 1995, **270**, 1789–1791.
- 11 K. Tajima, Y. Suzuki and K. Hashimoto, *J. Phys. Chem. C*, 2008, **112**, 8507–8510.
- 12 Y. Kim, S. Cook, S. M. Tuladhar, S. A. Choulis, J. Nelson, J. R. Durrant, D. D. C. Bradley, M. Giles, I. McCulloch, C. S. Ha and M. Ree, *Nat. Mater.*, 2006, **5**, 197–203.
- 13 L. Lu and L. Yu, *Adv. Mater.*, 2014, **26**, 4413–4430.
- 14 Z. He, B. Xiao, F. Liu, H. Wu, Y. Yang, S. Xiao, C. Wang, T. P. Russell and Y. Cao, *Nat. Photonics*, 2015, **9**, 174–179.
- 15 A. Mishra and P. Bauerle, *Angew. Chem., Int. Ed.*, 2012, **51**, 2020–2067.
- 16 S. D. Collins, N. A. Ran, M. C. Heiber and T.-Q. Nguyen, *Adv. Energy Mater.*, 2017, **7**, 1602242.
- 17 Y. Chen, X. Wan and G. Long, *Acc. Chem. Res.*, 2013, **46**, 2645–2655.
- 18 B. Kan, M. Li, Q. Zhang, F. Liu, X. Wan, Y. Wang, W. Ni, G. Long, X. Yang, H. Feng, Y. Zuo, M. Zhang, F. Huang, Y. Cao, T. P. Russell and Y. Chen, *J. Am. Chem. Soc.*, 2015, **137**, 3886–3893.
- 19 D. Deng, Y. Zhang, J. Zhang, Z. Wang, L. Zhu, J. Fang, B. Xia, Z. Wang, K. Lu, W. Ma and Z. Wei, *Nat. Commun.*, 2016, **7**, 13740.
- 20 Y. Lin, J. Wang, Z. Zhang, H. Bai, Y. Li, D. Zhu and X. Zhan, *Adv. Mater.*, 2015, **27**, 1170–1174.
- 21 Y. Yang, Z. Zhang, H. Bin, S. Chen, L. Gao, L. Xue, C. Yang and Y. Li, *J. Am. Chem. Soc.*, 2016, **138**, 15011–15018.
- 22 N. Qiu, H. Zhang, X. Wan, C. Li, X. Ke, H. Feng, B. Kan, H. Zhang, Q. Zhang, Y. Lu and Y. Chen, *Adv. Mater.*, 2017, **29**, 1604964.
- 23 S. Li, L. Zhan, F. Liu, J. Ren, M. Shi, C. Li, T. P. Russell and H. Chen, *Adv. Mater.*, 2018, **30**, 1705208.
- 24 J. Yuan, Y. Zhang, L. Zhou, G. Zhang, H.-L. Yip, T.-K. Lau, X. Lu, C. Zhu, H. Peng, P. A. Johnson, M. Leclerc, Y. Cao, J. Ulanski, Y. Li and Y. Zou, *Joule*, 2019, **3**, 1140–1151.
- 25 G. Zhang, J. Zhao, P. C. Y. Chow, K. Jiang, J. Zhang, Z. Zhu, J. Zhang, F. Huang and H. Yan, *Chem. Rev.*, 2018, **7**, 3447–3507.
- 26 B. Walker, A. B. Tomayo, X.-D. Dang, P. Zalar, J. H. Seo, A. Garcia, M. Tantiwivat and T.-Q. Nguyen, *Adv. Funct. Mater.*, 2009, **19**, 3063–3069.
- 27 Y. Sun, G. Welch, W. Leong, C. J. Takacs, G. C. Bazan and A. J. Heeger, *Nat. Mater.*, 2012, **11**, 44–48.
- 28 T. Lu and F. Chen, *J. Comput. Chem.*, 2012, **33**, 580–592.
- 29 J. Zhou, Y. Zuo, X. Wan, G. Long, Q. Zhang, W. Ni, Y. Liu, Z. Li, G. He, C. X. Li, B. Kan, M. Li and Y. Chen, *J. Am. Chem. Soc.*, 2013, **135**, 8484–8487.
- 30 Z. Li, G. He, X. Wan, Y. Liu, J. Zhou, G. Long, Y. Zuo, M. Zhang and Y. Chen, *Adv. Energy Mater.*, 2012, **2**, 74–77.
- 31 Q. Zhang, B. Kan, F. Liu, G. Long, X. Wan, X. Chen, Y. Zuo, W. Ni, H. Zhang, M. Li, Z. Hu, F. Huang, Y. Cao, Z. Liang, M. Zhang, T. P. Russell and Y. Chen, *Nat. Photonics*, 2015, **9**, 35–41.
- 32 K. Schulze, C. Urich, R. Schüppel, K. Leo, M. Pfeiffer, E. Brier, E. Reinold and P. Bäuerle, *Adv. Mater.*, 2006, **18**, 2872–2875.
- 33 R. Fitzner, E. Mena-Osteritz, A. Mishra, G. Schulz, E. Reinold, M. Weil, C. Koerner, H. Ziehlke, C. Elschner, K. Leo, M. Riede, M. Pfeiffer, C. Urich and P. Bäuerle, *J. Am. Chem. Soc.*, 2012, **134**, 11064–11067.

- 34 G. He, Z. Li, X. Wan, J. Zhou, G. Long, S. Zhang, M. Zhang and Y. Chen, *J. Mater. Chem. A*, 2013, **1**, 1801–1809.
- 35 B. Kan, Q. Zhang, M. Li, X. Wan, W. Ni, G. Long, Y. Wang, X. Yang, H. Feng and Y. Chen, *J. Am. Chem. Soc.*, 2014, **136**, 15529–15532.
- 36 K. Sun, Z. Xiao, S. Lu, W. Zajaczkowski, W. Pisula, E. Hanssen, J. M. White, R. M. Williamson, J. Subbiah, J. Ouyang, A. B. Holmes, W. W. H. Wong and D. J. Jones, *Nat. Commun.*, 2015, **6**, 6013.
- 37 Z. Zhou, S. Xu, J. Song, Y. Jin, Q. Yue, Y. Qian, F. Liu, F. Zhang and X. Zhu, *Nat. Energy*, 2018, **3**, 952–959.
- 38 R. Zhou, Z. Jiang, C. Yang, J. Yu, J. Feng, M. A. Adil, D. Deng, W. Zou, J. Zhang, K. Lu, W. Ma, F. Gao and Z. Wei, *Nat. Commun.*, 2019, **10**, 5393.
- 39 K. N. Winzenberg, P. Kemppinen, F. H. Scholes, G. E. Collis, Y. Shu, T. B. Singh, A. Bilic, C. M. Forsyth and S. E. Watkins, *Chem. Commun.*, 2013, **49**, 6307–6309.
- 40 Y. Kim, C. E. Song, S. J. Moon and E. Lim, *Chem. Commun.*, 2014, **50**, 8235–8238.
- 41 S. Li, L. Ye, W. Zhao, S. Zhang, S. Mukherjee, H. Ade and J. Hou, *Adv. Mater.*, 2016, **28**, 9423–9429.
- 42 W. Zhao, S. Li, H. Yao, S. Zhang, Y. Zhang, B. Yang and J. Hou, *J. Am. Chem. Soc.*, 2017, **139**, 7148–7151.
- 43 R. Mondal, S. Ko, J. E. Norton, N. Miyaki, H. A. Becerril, E. Verploegen, M. F. Toney, J.-L. Brédas, M. D. McGehee and Z. Bao, *J. Mater. Chem.*, 2009, **19**, 7195–7197.
- 44 L. Yuan, K. Lu, B. Xia, J. Zhang, Z. Wang, Z. Wang, D. Deng, J. Fang, L. Zhu and Z. Wei, *Adv. Mater.*, 2016, **28**, 5980–5985.
- 45 Z. Xiao, X. Jia and L. M. Ding, *Sci. Bull.*, 2017, **62**, 1562–1564.
- 46 C. Huang, X. Liao, K. Gao, L. Zuo, F. Lin, X. Shi, C.-Z. Li, H. Liu, X. Li, F. Liu, Y. Chen, H. Chen and A. K. Y. Jen, *Chem. Mater.*, 2018, **30**, 5429–5434.
- 47 W. Wang, B. Zhao, Z. Cong, Y. Xie, H. Wu, Q. Liang, S. Liu, F. Liu, C. Gao, H. Wu and Y. Cao, *ACS Energy Lett.*, 2018, **3**, 1499–1507.
- 48 Y. Liu, Z. Zhang, S. Feng, M. Li, L. Wu, R. Hou, X. Xu, X. Chen and Z. Bo, *J. Am. Chem. Soc.*, 2017, **139**, 3356–3359.
- 49 Z. Fei, F. D. Eisner, X. Jiao, M. Azzouzi, J. A. Rohr, Y. Han, M. Shahid, A. S. R. Chesman, C. D. Easton, C. R. McNeill, T. D. Anthopoulos, J. Nelson and M. Heeney, *Adv. Mater.*, 2018, **30**, 1705209.
- 50 X. Shi, L. Zuo, S. B. Jo, K. Gao, F. Lin, F. Liu and A. K. Y. Jen, *Chem. Mater.*, 2017, **29**, 8369–8376.
- 51 H. Feng, N. Qiu, X. Wang, Y. Wang, B. Kan, X. Wan, M. Zhang, A. Xia, C. Li, F. Liu, H. Zhang and Y. Chen, *Chem. Mater.*, 2017, **29**, 7908–7917.
- 52 B. C. Thompson and J. M. Frechet, *Angew. Chem., Int. Ed.*, 2008, **47**, 58–77.
- 53 J. L. Bredas, J. E. Norton, J. Cornil and V. Coropceanu, *Acc. Chem. Res.*, 2009, **42**, 1691–1699.
- 54 C. M. Proctor, M. Kuik and T.-Q. Nguyen, *Prog. Polym. Sci.*, 2013, **38**, 1941–1960.
- 55 G. Han and Y. Yi, *Adv. Theory Simul.*, 2018, **1**, 1800091.
- 56 S. M. Swick, W. Zhu, M. Matta, T. J. Aldrich, A. Harbuzaru, J. T. Lopez Navarrete, R. Ponce Ortiz, K. L. Kohlstedt, G. C. Schatz, A. Facchetti, F. S. Melkonyan and T. J. Marks, *Proc. Natl. Acad. Sci. U. S. A.*, 2018, **115**, E8341–E8348.
- 57 L. Zhu, Z. Tu, Y. Yi and Z. Wei, *J. Phys. Chem. Lett.*, 2019, **10**, 4888–4894.
- 58 S. Matthew Menke, Niva A. Ran, Guillermo C. Bazan and R. H. Friend, *Joule*, 2017, **2**, 25–35.
- 59 D. P. Qian, Z. L. Zheng, H. F. Yao, W. Tress, T. R. Hopper, S. L. Chen, S. S. Li, J. Liu, S. S. Chen, J. B. Zhang, X. K. Liu, B. W. Gao, L. Q. Ouyang, Y. Z. Jin, G. Pozina, I. A. Buyanova, W. M. Chen, O. Inganas, V. Coropceanu, J. L. Bredas, H. Yan, J. H. Hou, F. L. Zhang, A. A. Bakulin and F. Gao, *Nat. Mater.*, 2018, **17**, 703–709.
- 60 Z. Yao, X. Liao, K. Gao, F. Lin, X. Xu, X. Shi, L. Zuo, F. Liu, Y. Chen and A. K. Y. Jen, *J. Am. Chem. Soc.*, 2018, **140**, 2054–2057.
- 61 D. Baran, T. Kirchartz, S. Wheeler, S. Dimitrov, M. Abdelsamie, J. Gorman, R. S. Ashraf, S. Holliday, A. Wadsworth, N. Gasparini, P. Kaienburg, H. Yan, A. Amassian, C. J. Brabec, J. R. Durrant and I. McCulloch, *Energy Environ. Sci.*, 2016, **9**, 3783–3793.
- 62 W. R. Mateker and M. D. McGehee, *Adv. Mater.*, 2017, **29**, 1603940.
- 63 N. Li, J. D. Perea, T. Kassar, M. Richter, T. Heumueller, G. J. Matt, Y. Hou, N. S. Gueldal, H. W. Chen, S. Chen, S. Langner, M. Berlinghof, T. Unruh and C. J. Brabec, *Nat. Commun.*, 2017, **8**, 14541.
- 64 N. Gasparini, M. Salvador, S. Strohm, T. Heumueller, I. Levchuk, A. Wadsworth, J. H. Bannock, J. C. de Mello, H. J. Egelhaaf, D. Baran, I. McCulloch and C. J. Brabec, *Adv. Energy Mater.*, 2017, **7**, 1700770.
- 65 X. Du, T. Heumueller, W. Gruber, A. Classen, T. Unruh, N. Li and C. J. Brabec, *Joule*, 2019, **3**, 215–226.